

# Estimating Velocity and Attenuation Changes Due to CO<sub>2</sub> Saturation Using the Active Doublet Method: A Synthetic Study

Rong-Mao Zhou, Lianjie Huang, Peter Roberts, and James Rutledge  
Geophysics Group, MS D443  
Los Alamos National Laboratory  
Los Alamos, NM 87545

## ABSTRACT

Injection and movement/saturation of CO<sub>2</sub> in a geological formation will cause changes in seismic velocities and attenuation, which result in changes in seismic-wave scattering and propagation. Accurately estimating seismic velocity and attenuation changes from time-lapse seismograms will provide valuable information about where CO<sub>2</sub> moves. We conduct numerical studies of time-lapse seismic responses of CO<sub>2</sub> injection with different saturation levels of CO<sub>2</sub>, using a finite-difference elastic-wave equation scheme. The method has the fourth-order accuracy in space and the second-order accuracy in time. A reference layered model (P-wave velocity:  $V_P$ ; S-wave velocity:  $V_S$  and density:  $\rho$ ) is chosen based on the elastic Marmousi model for synthetic seismogram calculations. The active doublet method is used to estimate changes in seismic velocities and attenuation using synthetic time-lapse vertical seismic profiling (VSP) data. Synthetic seismograms are calculated using three sets of test models, in which velocities and/or attenuation within a layer are perturbed. We use two test models containing only velocity changes, three test models having only attenuation changes, and one test model with changes in both velocities and attenuation. We conduct active doublet analyses on perturbed and unperturbed seismograms recorded at receivers located at different distances from the perturbed layer. Because the method averages the perturbation effects over entire wave-propagation paths from a source to a receiver, the estimated velocity changes are largest at the receiver closest to the perturbed layer and smallest at the furthest receiver. However, estimates of attenuation changes show no such correlation with the receiver proximity.

## INTRODUCTION

Geological sequestration involves storing large quantities of CO<sub>2</sub> within underground rock formations for long periods of time, and seismic monitoring could be an important tool to ensure safe storage of CO<sub>2</sub>. Depleted oil reservoirs, saline aquifers, and un-mineable coal seams have been suggested as storage sites. The CO<sub>2</sub> could be held within the rock pore spaces. These pore spaces have previously held oil/natural gas/water for millions of years.

Rock and fluid physics measurements and modeling suggest that CO<sub>2</sub> can cause a 4-6% decrease in P-wave velocity and a 5-10% change in S-wave velocity (Davie *et al.*, 2003). Time-lapse VSP surveys for monitoring CO<sub>2</sub> sequestration also showed P-wave and S-wave velocity changes due to CO<sub>2</sub> injection and strong reflections from injection regions (Arts *et al.*, 2004; Daley *et al.*, 2005).

Wang *et al.* (1998) investigated the effect of CO<sub>2</sub> floods on the seismic velocities in a carbonate rock (dolostone). They found that  $V_P$  decreases from a minimum 3% to as high as 10.9%, while  $V_S$  decreases from 3.3% to 9.5% as the reservoir rocks are flooded with CO<sub>2</sub> under in-situ conditions. Their results show that the combined effects of pore pressure buildup and fluid substitution caused by CO<sub>2</sub> flooding make it petrophysically feasible to monitor the CO<sub>2</sub> flood process and to map the flooded zones seismically.

The attenuation of compressional and shear waves in rocks strongly depends on the physical state and saturation conditions. Observations show that attenuation for fluid-saturated rocks is higher than for dry rocks, depends on the degree of saturation and fluid type, and decreases with increasing confining pressure. Studies also indicate that compressional attenuation is greater than shear attenuation in partially saturated rock, and the reverse is true in fully saturated rock (White, 1975; Toksoz *et al.*, 1979; Johnson *et al.*, 1979; Hauge, 1981; Winkler and Nur, 1982; Klimentos, 1995; Schütt *et al.*, 2005).

The usefulness of temporal changes, however, is limited by the accuracy and precision with which velocity and attenuation measurements can be made (Roberts *et al.*, 1992). Poupinet *et al.* (1984) presented a high-precision method for measuring temporal velocity changes in the Earth's crust. These studies indicate that, with sufficiently precise recording equipment, measurements of velocity changes on

the order of 0.01% could be made.

In this study, we calculate numerical time-lapse seismic responses due to CO<sub>2</sub> injection using a finite-difference elastic-wave equation scheme. The method has the fourth-order accuracy in space and the second-order accuracy in time (Cheng, 1994; Kamm *et al.*, 1996). We use the active doublet method developed by Poupinet *et al.* (1984), with improvements made by Roberts *et al.* (1992), to estimate small changes in seismic velocities and attenuation using synthetic time-lapse VSP data. A similar method was later published by Snieder *et al.* (2002) and called “code-wave interferometry”.

## METHODOLOGY

The basic method of doublet phase analysis, as originally described by Poupinet *et al.* (1984), involves incrementing a data window through both doublet signals simultaneously. A Fast Fourier Transform (FFT) is then computed for each windowed signal at each time step. For each pair of data windows, the cross spectrum is obtained by multiplying the Fourier transform of one signal by the complex conjugate of the other:

$$S_{12}(t, f) = S_1(t, f)S_2^*(t, f) \quad (1)$$

Where  $S_1(t, f)$  and  $S_2(t, f)$  are the Fourier transforms of the two windowed signals at elapsed time  $t$ ,  $S_{12}(t, f)$  is their cross spectrum, and the asterisk indicates the complex conjugate, and  $f$  is the frequency. The phase  $\phi$  of  $S_{12}$  for progressively later time windows is used to obtain the relative signal delay as a function of elapsed time, beginning at the first arrival and extending through the coda. This, in turn, leads to estimates of relative changes in velocity,  $\Delta V/V$ , if the signal delay versus elapsed time follows a linear relation over some portion of the coda. If the linear trend persists over the entire coda, then the velocity change is pervasive throughout the sampled volume. The original method of Poupinet *et al.* (1984) fails to take full advantage of the principal assumption that, as long as dispersion and mixed wave type effects are negligible, the cross-spectral phase is linear with a value of zero at the intercept. This assumption allows us to eliminate the intermediate phase regression steps so that, instead of estimating a single delay point for each time window, we convert all phase data to units of equivalent time delay as equation (2):

$$\tau(t, f) = \frac{\phi(t, f)}{2\pi f} \quad (2)$$

All phase-derived time delays are then plotted directly versus elapsed time. In this way, all usable phase data may be fit simultaneously to obtain  $\Delta V/V$  in one step rather than two. This allows trends in the measure delays to be derived from the cross-spectral phase directly rather than from intermediate measurements based on the slope of the  $\phi$  vs.  $f$  curves. This is particularly useful for reducing errors caused by erratic phase data at lower frequencies when dealing with narrow-band data (Roberts *et al.*, 1992).

Extending the doublet algorithm to obtain changes in  $\Delta Q^{-1}$  involves calculating spectral amplitude ratios for the same data window pairs that are used to obtain cross-spectral phase.  $Q$  is the quality factor, and  $\Delta Q^{-1}$  is proportional to the attenuation change. After taking the natural logarithm of the spectral ratios and scaling by  $f$ , all data may be plotted simultaneously versus elapsed time, similar to the way the phase-derived time delays are treated. The scaled spectral ratios can be represented as a function of elapsed time by:

$$\ln \left[ \frac{\|S_1(t, f)\|}{\|S_2(t, f)\|} \right] \frac{1}{f} = \frac{\ln[R_0(f)]}{f} + \pi t \Delta Q^{-1} \quad (3)$$

Where  $S_1(t, f)$  and  $S_2(t, f)$  are the Fourier transforms versus elapsed time of the numerator and denominator signals, respectively, and  $R_0 = \|S_1(0, f)\|/\|S_2(0, f)\|$  is the relative source term which, in the case of true doublets, should be unity. The slope of a regression line fit to data that obey this relation is proportional to  $\Delta Q^{-1}$ . More details about the amplitude-decay methodology can be found in Roberts *et al.* (1992).

## VELOCITY MODELS AND SYNTHETIC SEISMOGRAMS

In this study, we used a layered elastic model ( $V_p$ ,  $V_s$  and  $\rho$ ) to calculate the synthetic VSP seismograms (Fig. 1). The layered model was based on the Marmousi 2 model (Martin et al., 2006) without the top water layer and with the thickness of the reservoir layer increased from 120m to 200m at the depth range of 1360 to 1560m (the reference model).

Figure 2 illustrates VSP source and receiver geometries for the synthetic seismogram calculations. The red asterisk denotes the source, blue triangles are receivers, and the green filled rectangle represents the reservoir layer with a thickness of 200m from depth 1360m. The VSP offset is 1000m and the source is located at 50m below surface.

A finite-difference elastic-wave-equation scheme was used to calculate synthetic seismograms. The method has the fourth-order accuracy in space and the second-order accuracy in time (Cheng, 1994; Kamm *et al.*, 1996). Figure 3 shows horizontal and vertical seismograms calculated using an explosive point source with a center frequency of 50Hz. Figure 4 shows the separate P- and S-waves calculated from the dilatation and rotation (Sun and McMechan, 2001), respectively, of the wavefield. Upgoing and downgoing P-wave and S-wave separation is accomplished in the frequency-wavenumber ( $f-k$ ) domain using the technique of contour-slice filtering (Suprajitno and Greenhalgh, 1985; Hardage, 2000) (Figure 5). Only the upgoing P-waves were used for active doublet analysis.

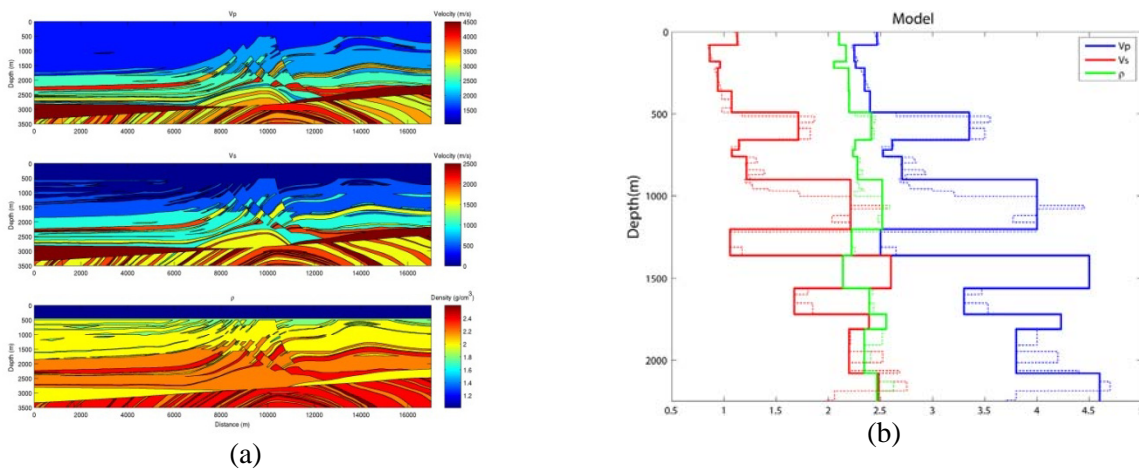


Figure 1. Shown in (a) is the elastic Marmousi model ( $V_p$ ,  $V_s$  and  $\rho$ ). Depicted in (b) is a profile of the elastic Marmousi model at 12000m (thin dotted lines) and a modified layered model (thick solid lines) used for synthetic seismogram calculations.

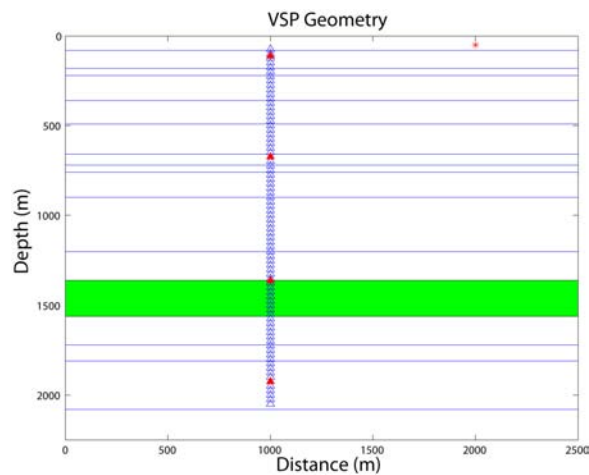


Figure 2. VSP geometry used for synthetic seismogram calculations. The red asterisk denotes the source and blue triangles are receivers. Active doublet data analyses are conducted at four receivers (from top to bottom: #50, 500, 1050, 1500) marked as red solid triangles.

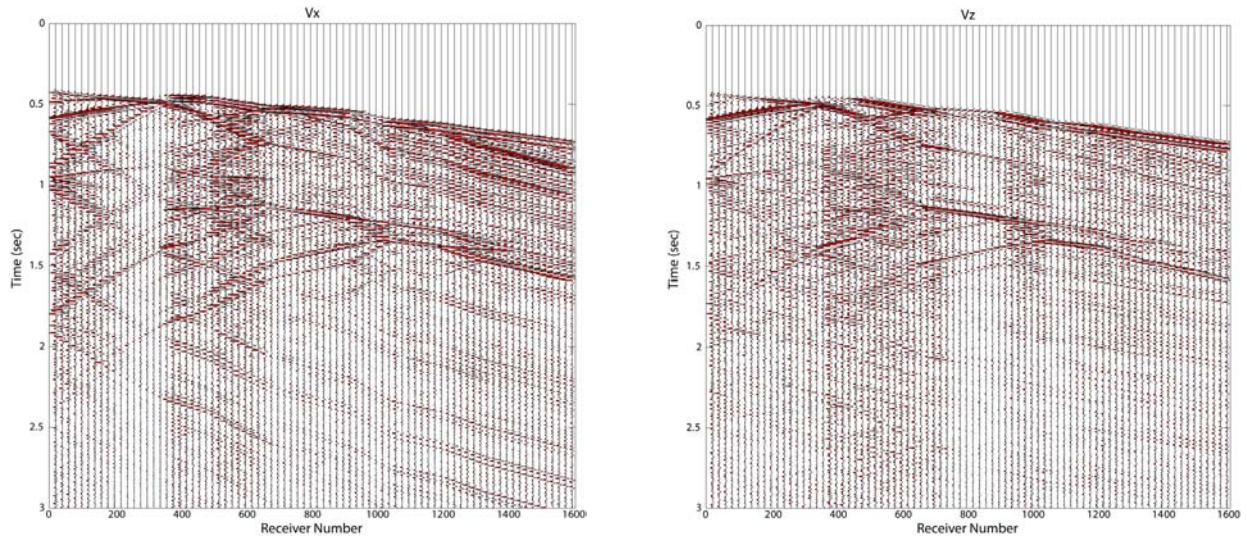


Figure 3. Synthetic VSP seismogram (Left: Vx; Right Vz).

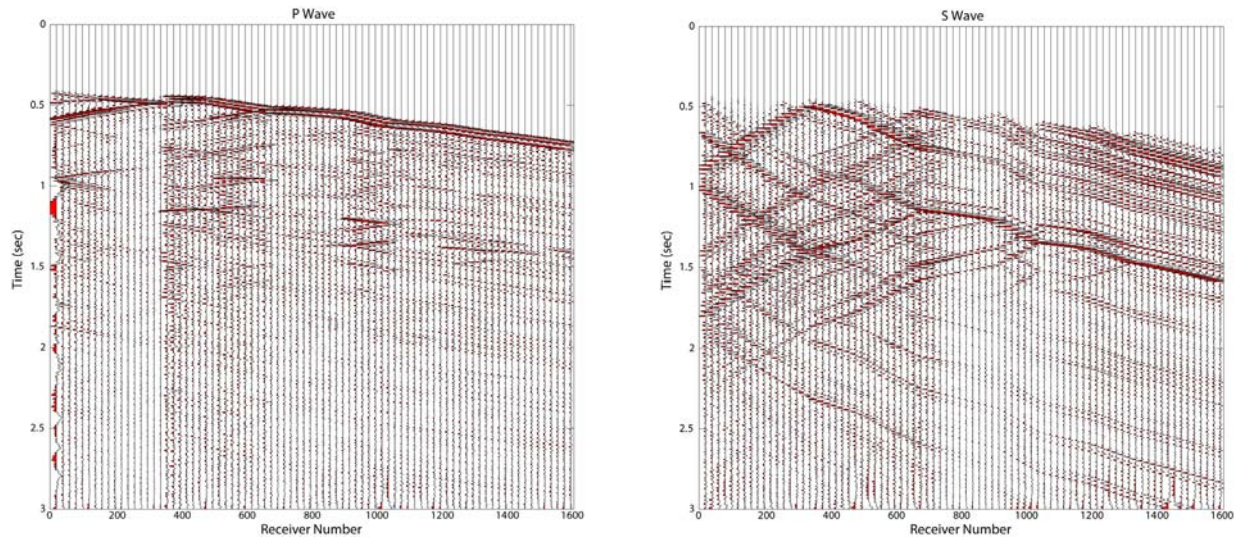


Figure 4. Separated P-wave (Left) and S-wave (Right) VSP seismograms.

Rock and fluid physics measurements and modeling suggest that  $\text{CO}_2$  can cause a 4-6% decrease in P-wave velocity and a 5-10% decrease in S-wave velocity (Davie *et al.*, 2003). To test the active doublet method for estimating  $\text{CO}_2$ -induced changes in seismic velocities and attenuation using synthetic time-lapse VSP data, synthetic seismograms were calculated using different test models and compared with those calculated from the reference model (Fig. 1). Test model 1 had 6% P-wave velocity decrease and 5% S-wave velocity decrease in the reservoir layer (green layer in Fig. 2) relative to the reference model; Test model 2 had 3% P-wave velocity decrease and 2.5% S-wave velocity decrease relative to the reference model. Neither test model 1 or test model 2 included attenuation. Test model 3 includes attenuation ( $Q^{-1}=0.02$ ) in the reservoir layer and has the same velocities as the reference model. Test model 4 ( $Q^{-1}=0.05$ ) and 5 ( $Q^{-1}=0.04$ ) have different  $Q$  but the same velocities as model 3. Test model 6 had  $Q^{-1}=0.05$  and the same velocities as test model 1. The parameters of these models are summarized in Table 1. Figure 6 shows upgoing P-wave synthetic seismograms at receivers #50, #500, #1050, and #1500 for the reference model overlaid with their counterpart doublet seismograms for the different test models.

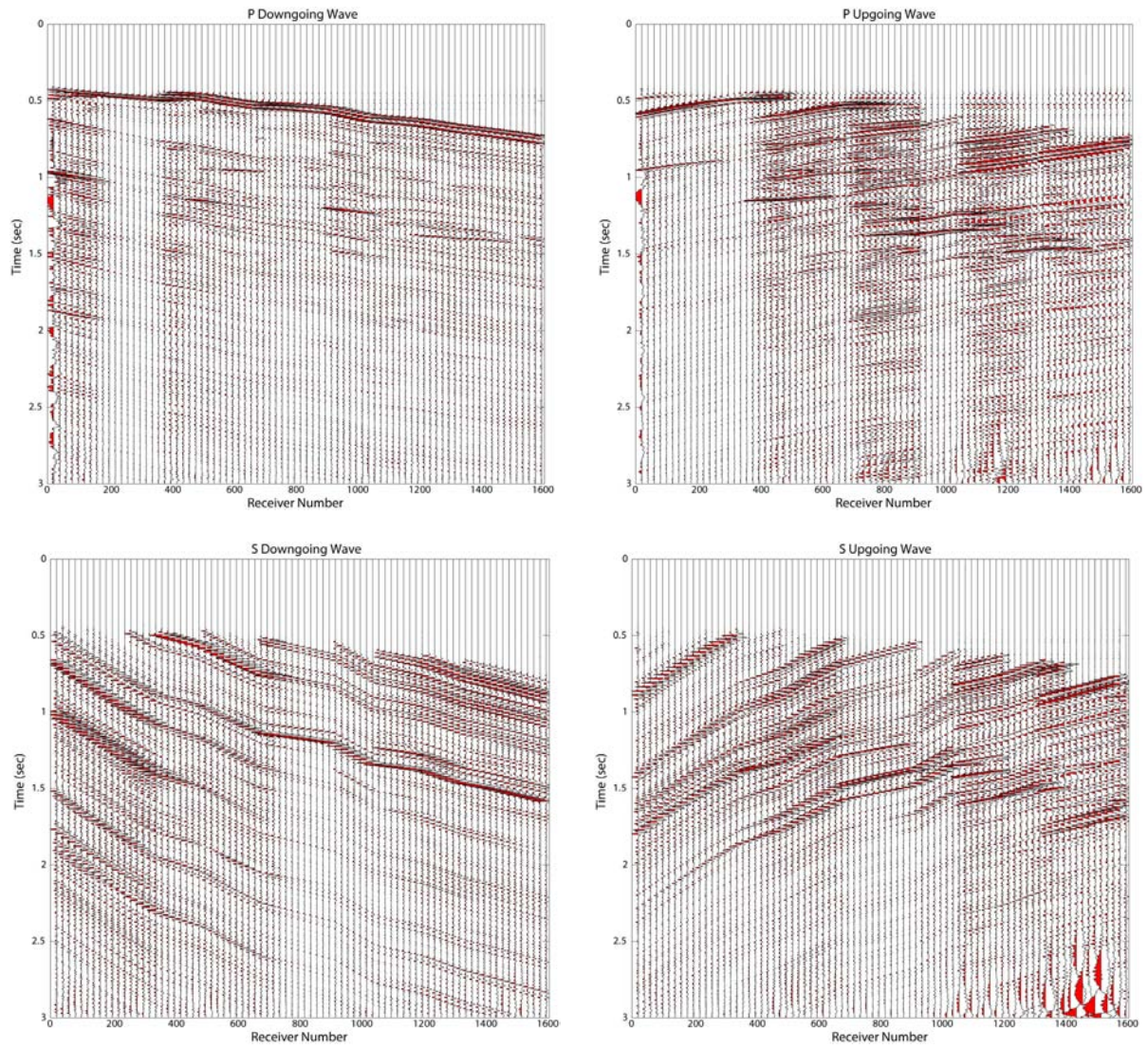


Figure 5. Downgoing and upgoing VSP seismograms separated using the  $f$ - $k$  analysis.

**Table 1. Model parameters for synthetic seismogram calculations**

Model Code	$V_P$ (km/s)	$V_S$ (km/s)	$Q^{-1}$
Reference Model	4.5	2.6	None
Test Model 1	4.23	2.47	None
Test Model 2	4.365	2.535	None
Test Model 3	4.5	2.6	0.02
Test Model 4	4.5	2.6	0.05
Test Model 5	4.5	2.6	0.04
Test Model 6	4.23	2.47	0.05

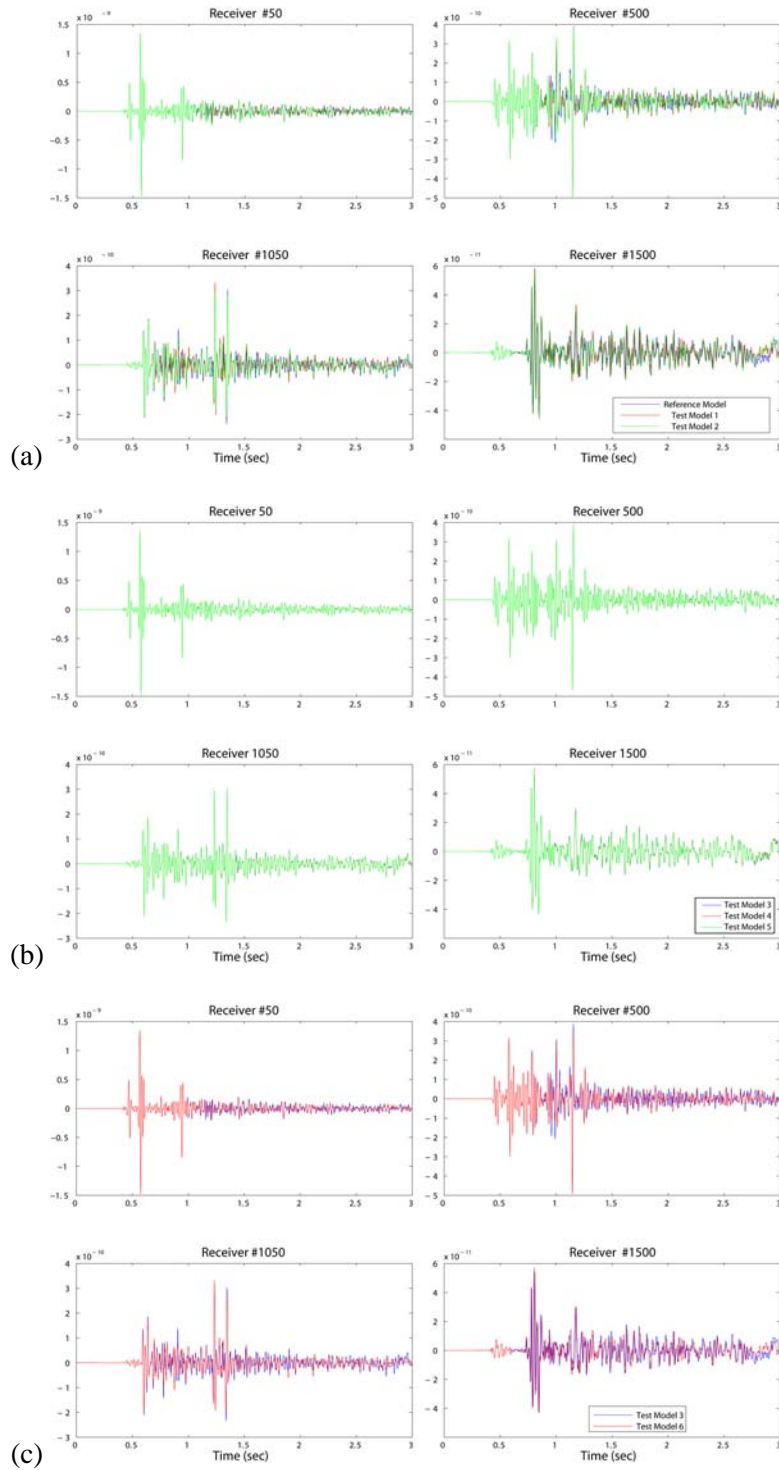


Figure 6. Overlaid upgoing P-wave synthetic seismograms at 4 receivers (#50, #500, #1050 and #1500) for different models: (a) comparison of synthetic seismograms for the reference model (blue), test model 1 (-6% change in  $V_p$ , -5% change in  $V_s$ ) (red) and test model 2 (-3% change in  $V_p$ , -2.5% change in  $V_s$ ); (b) same as (a) but for test model 3 ( $Q^{-1}=0.02$ ), test model 4 ( $Q^{-1}=0.05$ ) and test model 5 ( $Q^{-1}=0.04$ ); (c) same as (a) and (b) but for test model 3 (blue) ( $Q^{-1}=0.02$ ) and test model 6 ( $Q^{-1}=0.05$ , -6% change in  $V_p$  and -5% change in  $V_s$ ).

## ACTIVE DOUBLET DATA ANALYSIS

Figures 7-11 show the results of doublet phase and amplitude analyses applied to upgoing P-wave synthetic seismograms at four receivers (#50, #500, #1050, and #1500). Figure 7 shows the results of doublet phase analysis for test model 1 (-6% change in  $V_p$  and -5% change in  $V_s$ ) relative to the reference model. The measured values show that  $\Delta V/V$  are larger for receivers that are closer to the reservoir layer, reaching a maximum of 1.24% at receiver #1050, which is located at the top of the reservoir layer. Figure 8 shows similar results for test model 2 (-3% change in  $V_p$  and -2.5% change in  $V_s$ ). Although volume-averaging and multiple-reflection effects cause the doublet velocity changes to be smaller than the actual test-model values relative to the reference model, the doublet velocity change in Fig. 8 is about half that in Fig. 7 for each receiver. This is consistent with the actual relative changes between test model 1 and test model 2. These results demonstrate the robustness of the doublet phase analysis technique and its sensitivity to relative velocity changes.

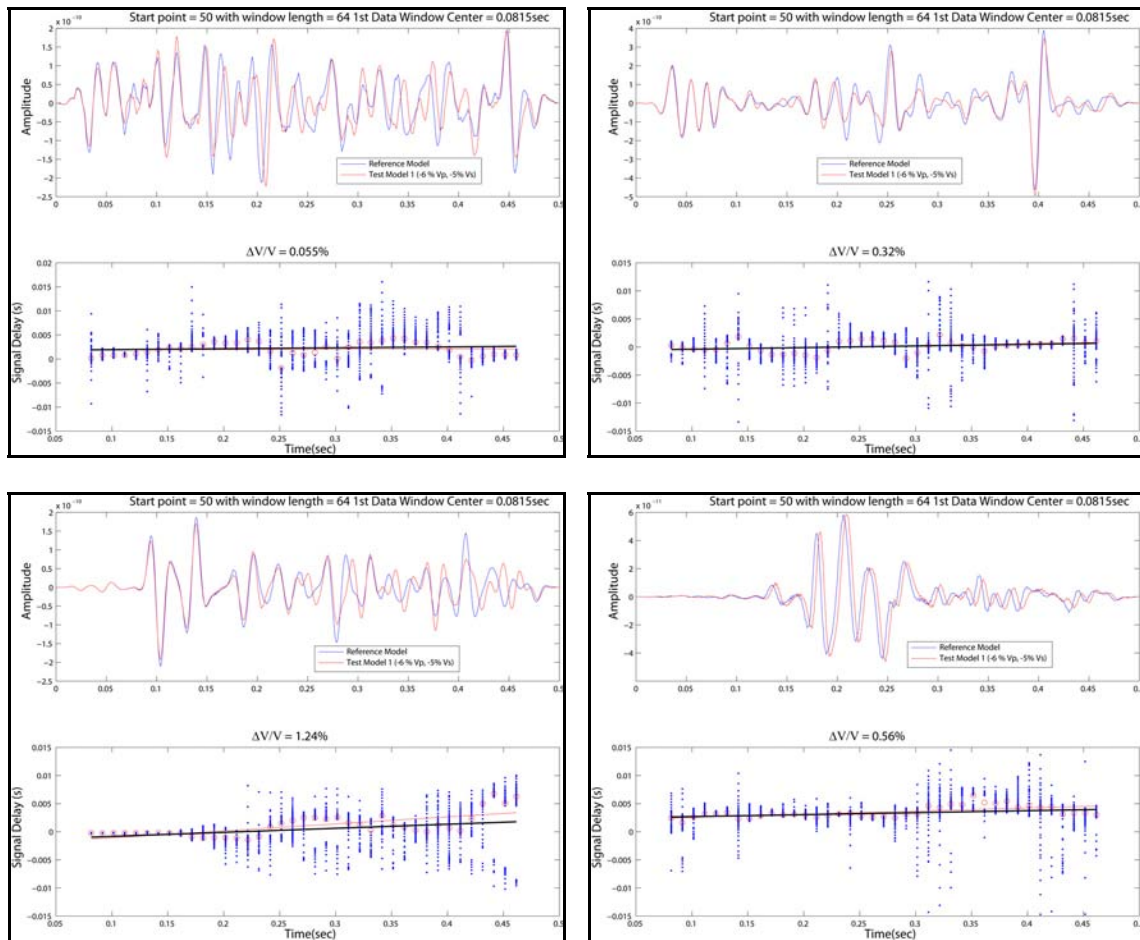


Figure 7. Results of doublet phase analysis for synthetic seismograms for the reference model and test model 1 (-6% change in  $V_p$  and -5% change in  $V_s$  relative to the reference model) at four receivers (Upper left: # 50; Upper right: # 500; Lower left: # 1050; and Lower right: #1500). For each receiver, the top sub-panel is the plot of the synthetic seismograms used for phase analysis and the bottom sub-panel is the plot of signal delay versus elapsed time. Red circles mark the median phase values at each elapsed time and the red line is the least-squares fit of the delays for these median phases. The black line is the fit of the delays for all phases at all elapsed times and its slope gives the value of the velocity change,  $\Delta V/V$ .

Figure 9 illustrates the results of double amplitude analysis for test model 3 ( $Q^{-1} = 0.02$ ) relative to test model 4 ( $Q^{-1} = 0.05$ ). Figure 10 shows the results for test model 3 relative to test model 5 ( $Q^{-1} = 0.04$ ). The changes in  $Q^{-1}$  show similar characteristics as the previous velocities changes in that  $\Delta Q^{-1}$  is largest for receivers closest to the reservoir layer. However, there is no direct correlation of these changes with distance from the reservoir, as with the velocity changes. Although the velocities in test model 3 and test model 4 are identical, Figures 9 and 10 show doublet phase analyses still yield  $\Delta V/V$ 's of 0.01% or less. This might be caused by numerical errors in the synthetic seismogram calculations or it could be caused by phase differences introduced by attenuation.

We used the active doublet method to analyze synthetic time-lapse VSP seismograms for models with changes both in velocities and attenuation. Test model 3 had  $Q^{-1}=0.02$  with same velocity as the reference model, and test model 6 had  $Q^{-1}=0.05$ , -6% change in  $V_P$  and -5% change in  $V_S$  relative to the reference model. Figure 11 shows the results for the four receivers (#50, #500, #1050 and #1500).

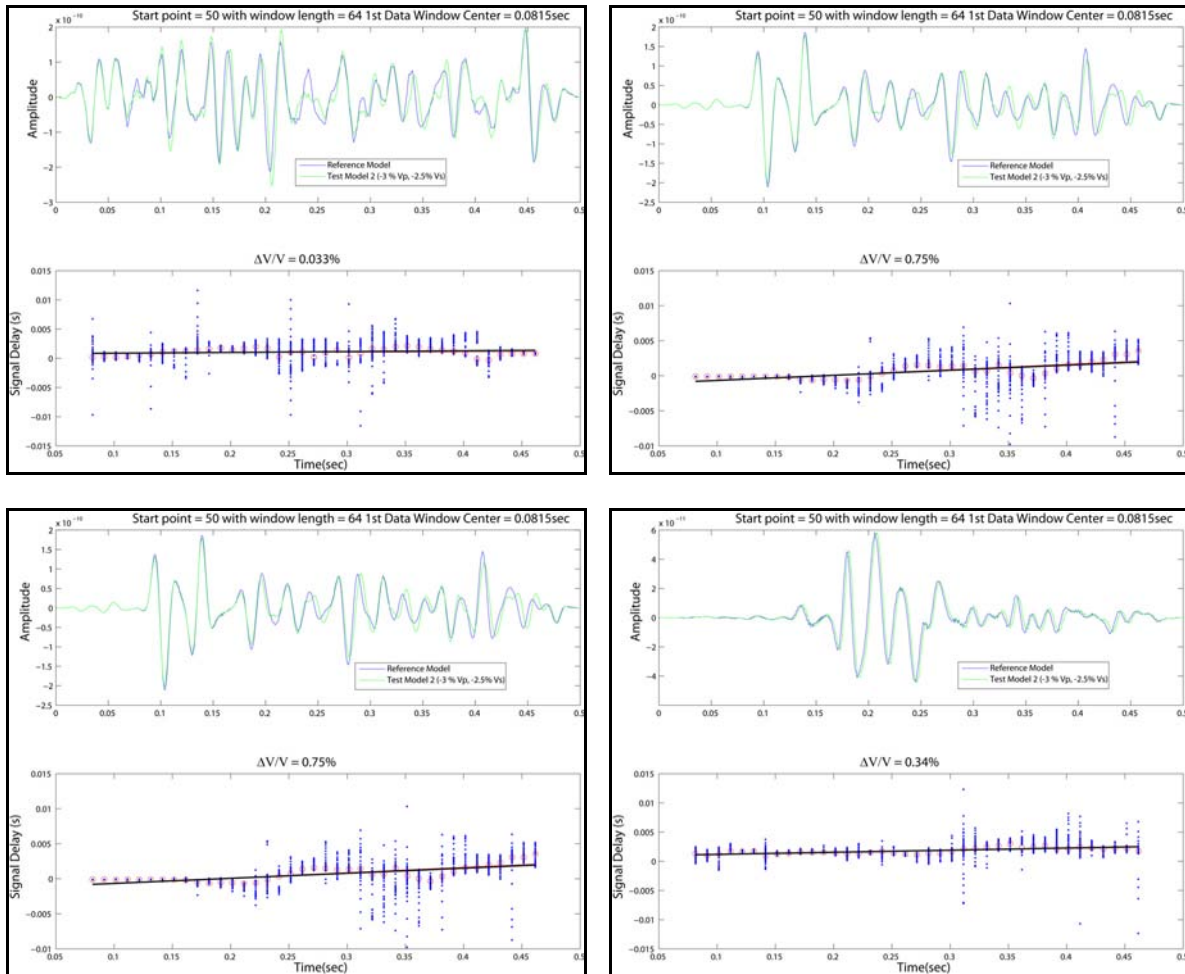


Figure 8. Results of doublet phase analysis for synthetic seismograms for the reference model and test model 2 (-3% change in  $V_p$  and -2.5% change in  $V_s$  relative to the reference model) at four receivers (Upper left: # 50; Upper right: # 500; Lower left: # 1050; and Lower right: #1500). Plotting conventions are the same as Fig. 7.

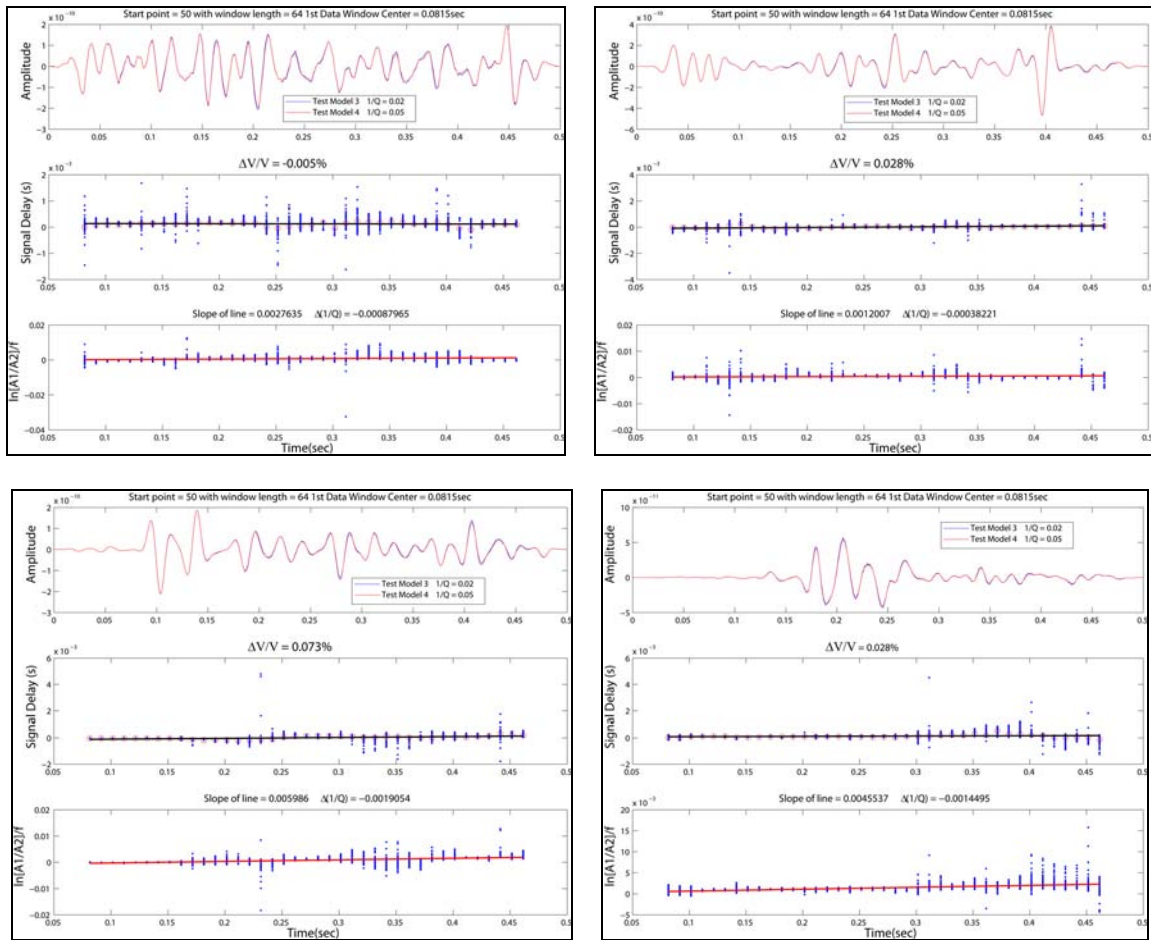


Figure 9. Results of doublet phase and amplitude analyses for test model 3 ( $Q^{-1} = 0.02$ ) relative to test model 4 ( $Q^{-1} = 0.05$ ) at four receivers (Upper left: # 50; Upper right: # 500; Lower left: # 1050; and Lower right: #1500). For each receiver, the top sub-panel shows synthetic seismograms; the mid sub-panel shows signal delay versus elapsed time as in Figs. 7 and 8; the bottom sub-panel shows scaled amplitude ratios versus elapsed time. The red line is the least-squares fit and its slope divided by  $\pi$  gives the attenuation change,  $\Delta Q^{-1}$ .

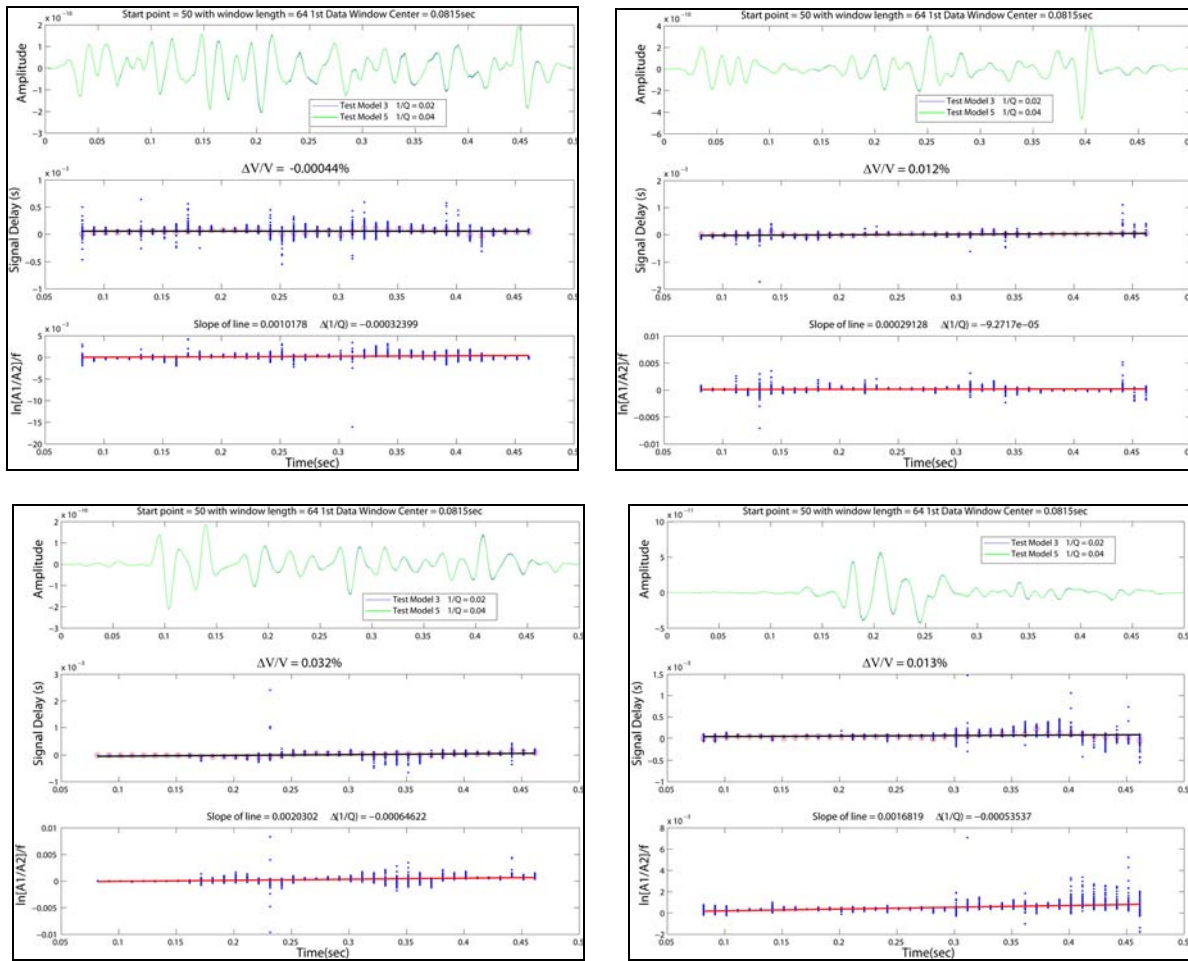


Figure 10. Results of doublet phase and amplitude analyses for test model 3 ( $Q^{-1} = 0.02$ ) relative to test model 5 ( $Q^{-1} = 0.04$ ) at four receivers (Upper left: # 50; Upper right: # 500; Lower left: # 1050; and Lower right: #1500). Plotting conventions are the same as in Fig. 9.

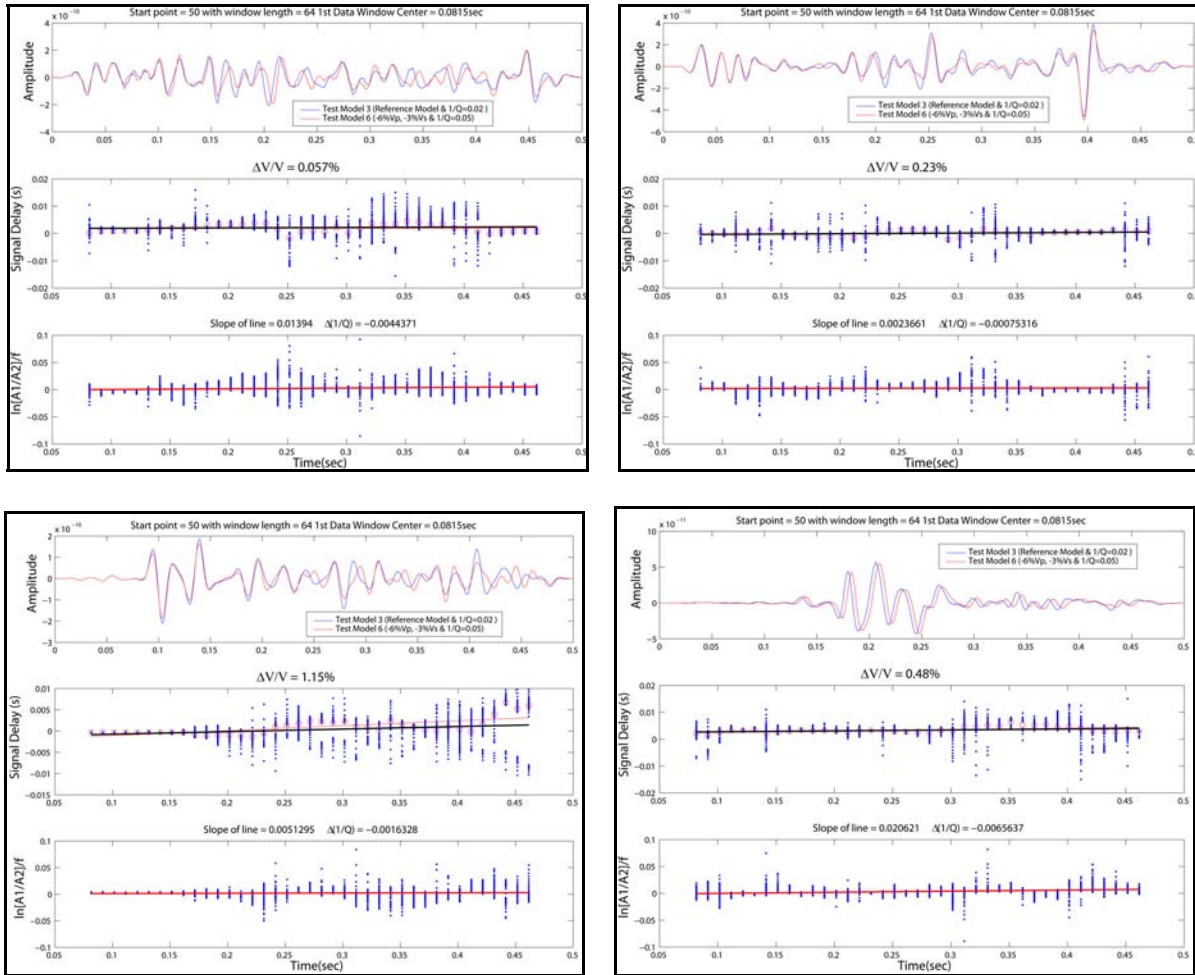


Figure 11. Results of doublet phase and amplitude analysis for test model 3 ( $Q^{-1}=0.02$ ) relative to test model 6 ( $Q^{-1}=0.05$ , -6% change in  $V_p$  and -5% change in  $V_s$ ) at four receivers (Upper left: # 50; Upper right: # 500; Lower left: # 1050; and Lower right: #1500). Plotting conventions are the same as in Figure 9.

## CONCLUSIONS

We have investigated the active doublet method for estimating velocity and attenuation changes using time-lapse VSP synthetic seismograms. We tested three kinds of structural models that include either velocity changes or attenuation changes, or both. The phase-delay analysis shows that  $\Delta V/V$  is largest for receivers closest to the reservoir layer, reaching a maximum at the receiver near the top of the reservoir layer. The amplitude ratio analysis shows that attenuation changes at different receivers have no correlation with the distance between the receivers and reservoir.

## ACKNOWLEDGEMENT

This work is supported by the US Department of Energy's Southwest Regional Partnership on Carbon Sequestration.

## REFERENCES

- Arts, R., O. Eiken, A. Chadwick, P. Zweigel, L. van der Meer, and B. Zinszner (2004). Monitoring of  $\text{CO}_2$  injected at Sleipner using time-lapse seismic data. *Energy* **29**, 1383-1392.
- Cheng, N. (1994). Borehole wave propagation in isotropic and anisotropic media: three-dimension finite difference approach, *Ph.D. Thesis*, Massachusetts Institute of Technology.
- Davis, T. L., M. J. Terrell, R. D. Benson, R. Cardona, R. R. Kendall and R. Winarsky (2003). Multicomponent seismic characterization and monitoring of  $\text{CO}_2$  flood at Weyburn Field,

- Saskatchewan. *The Leading Edge* **22**, 696-697.
- Daley, T.M, L.R. Myer, E.L. Majer, J.E. Peterson (2005). Acquisition of time-lapse, 6-component, P- and S-wave, crosswell seismic survey with orbital vibrator, and of time-lapse VSP for CO<sub>2</sub> injection monitoring. In *Expanded Abstracts*, 75<sup>th</sup> Ann. Internat. Mtg., Soc. Expl. Geophys., Houston, Texas, 1277-1279.
- Hardage, B. A. (2000). *Handbook of Geophysical Exploration*, Vol. 14: Vertical seismic profiling: principles, third updated and revised edition, Elsevier Science Ltd.
- Hauge, P. S. (1981). Measurements of attenuation from vertical seismic profiles. *Geophysics* **46**, 1548-1558.
- Johnston, D. H. , Toksöz, M. N., and A. Timur (1979). Attenuation of seismic waves in dry and saturated rocks, Part I: Mechanisms. *Geophysics* **44**, 691-711.
- Kamm, J. R., R. J. Bos, and E. M. Jones (1996). User's Guide to AFD v. 1.0. Los Alamos National Laboratory, LA-UR-96-853.
- Klimentors, T. (1995). Attenuation of P- and S-waves as a method of distinguishing gas and condensate from oil and water. *Geophysics* **60**, 447-458.
- Martin, G. S., R. Wiley and K. J. Marfurt (2006). Marmousi2: An elastic upgrade for Marmousi. *The Leading Edge*. 156-166
- Poupinet, G., W. L. Ellsworth, and J. Frechet (1984). Monitoring velocity variation in the Crust using earthquake doublets: an application to the Calaveras Fault, California, *J. Geophys. Res.* **89**, 5719-5731.
- Roberts, P. M., W. S. Phillips, and M. C. Fehler (1992). Development of the active doublet method for measuring small velocity and attenuation changes in solids, *J. Acoust. Soc. Am.* **91**(6), 3291-3302.
- Schütt, H., M. Wigand, and E. Spangenberg (2005). Geophysical and geochemical effects of supercritical CO<sub>2</sub> on sandstones. In the *Carbon Dioxide Capture for Storage in Deep Geologic Formations*, Vol. 2 (eds. D. C. Thomas and S. M. Benson), Elsevier, 767-786.
- Snieder, R., A. Grêt, H. Douma, and J. Scales (2002). Coda wave interferometry for estimating nonlinear behavior in seismic velocity, *Science* **295**, 2253-2255.
- Sun, R. and G. A. McMechan (2001). Scalar reverse-time depth migration of prestack elastic seismic data. *Geophysics* **66**, 1519-1527.
- Suprajitno, M. and S. A. Greenhalgh (1985). Separation of upgoing and downgoing waves in vertical seismic profiling by contour-slice filtering. *Geophysics* **50**, 950-962.
- Toksöz, M. N., D. H. Johnston, and A. Timur (1979). Attenuation of seismic waves in dry and saturated rocks, Part I: Laboratory measurements. *Geophysics* **44**, 681-690.
- Wang, Z., M. E. Cates, and R. L. Langan (1998). Seismic monitoring of CO<sub>2</sub> flood in a carbonate reservoir: A rock physics study, *Geophysics* **63**, 1604-1617.
- White, J. E. (1975). Computed seismic speeds and attenuation in rocks with partial gas saturation. *Geophysics* **40**, 224-232.
- Winkler, K. W. and A. Nur (1982). Seismic attenuation: effects of pore fluids and frictional sliding. *Geophysics* **47**, 1-15.